J Mater Sci: Mater Electron (2015) 26:4078–4084
DOI 10.1007/s10854-015-2947-x

$Y_2O_2S:Yb^{3+}$, Er^{3+} nanofibers: novel fabrication technique, structure and up-conversion luminescent characteristics

Xin Lu[1,2] · Ming Yang[3] · Liying Yang[3] · Qianli Ma[3] · Xiangting Dong[3] · Jian Tian[1]

Received: 11 February 2015 / Accepted: 12 March 2015 / Published online: 22 March 2015

Abstract $Y_2O_3:Yb^{3+}$, Er^{3+} nanofibers were prepared by calcination of the electrospun polyvinyl pyrrolidone (PVP)/$[Y(NO_3)_3 + Yb(NO_3)_3 + Er(NO_3)_3]$ composite nanofibers. For the first time, $Y_2O_2S:Yb^{3+}$, Er^{3+} up-conversion luminescent nanofibers were successfully synthesized via inheritance of the morphology and sulfurization of the above electrospinning-derived $Y_2O_3:Yb^{3+}$, Er^{3+} nanofibers using sulfur powders as sulfur source by a double-crucible method we newly proposed. XRD analysis indicates that $Y_2O_2S:Yb^{3+}$, Er^{3+} nanofibers are pure hexagonal in structure with space group $P\bar{3}m1$. Observation results of FESEM and TEM reveal that the diameters of $Y_2O_2S:Yb^{3+}$, Er^{3+} nanofibers are 105 ± 13 nm, and $Y_2O_2S:Yb^{3+}$, Er^{3+} nanofibers are composed of nanoparticles with the diameter ranging from 40 to 70 nm. Up-conversion emission spectrum analysis manifests that $Y_2O_2S:Yb^{3+}$, Er^{3+} nanofibers exhibit strong green and red up-conversion emission centering at 526, 548 and 668 nm, respectively. The green emissions and the red emission are respectively assigned to $^2H_{11/2}/^4S_{3/2} \rightarrow {}^4I_{15/2}$ and $^4F_{9/2} \rightarrow {}^4I_{l5/2}$ energy levels transitions of Er^{3+} ions. The formation mechanism of $Y_2O_2S:Yb^{3+}$, Er^{3+} upconversion luminescence nanofibers is also proposed. More importantly, this new strategy and fabrication technique are of universal significance to prepare other rare earth oxysulfides with various morphologies.

1 Introduction

As a group of important wide-gap (4.6–4.8 eV) semiconductors, rare earth oxysulfides with high chemical and thermal stability have been extensively used as luminescent matrix owing to their high absorption of light and energy transfer efficiency, and have become one of the major optical functional materials [1, 2]. Especially, rare earth ions activated rare earth oxysulfides have become a very important family of inorganic phosphor materials [3]. Upconversion (UC) luminescence nanophosphors doped with trivalent rare earth ions have attracted considerable interests [4, 5]. As the candidate of upconversion nanomaterial, Y_2O_2S nanocrystals doped with Er^{3+} ions and sensitized by Yb^{3+} ions have been extensively studied, the sensitizer is excited by an infrared radiation (IR) source and the energy is transfered to the activator that emits a visible photon. Generally, Er^{3+} ion serves as luminescence center owing to its abundant energy levels and narrow emission spectral lines [6, 7], and it is in perfect agreement with the energy levels of Yb^{3+} ion absorption [8]. Recently, a large number of fabrication methods have already been employed to fabricate nano- and microsized $Y_2O_2S:Yb^{3+}$, Er^{3+}, such as hydrothermal and solvothermal methods [9], solid sate reaction method [10, 11], combustion method [12, 13], microwave-heating method [14, 15], etc. These methods are usually used to produce nanoparticles, nanotubes, nanowires, nanorods and nanoflowers [16–18]. In order to obtain a new morphology of

✉ Xiangting Dong
dongxiangting888@163.com

✉ Jian Tian
tianjian@cust.edu.cn

[1] Clean Energy Technology Laboratory, Changchun University of Science and Technology, Changchun 130022, China

[2] School of Sciences, Changchun University, Changchun 130022, China

[3] Key Laboratory of Applied Chemistry and Nanotechnology at Universities of Jilin Province, Changchun University of Science and Technology, Changchun 130022, China

$Y_2O_2S:Yb^{3+}$, Er^{3+} nanomaterial, fabrication of $Y_2O_2S:Yb^{3+}$, Er^{3+} upconversion luminescent nanofibers is a meaningful subject of study. To our knowledge, no reports on $Y_2O_2S:Yb^{3+}$, Er^{3+} upconversion luminescent nanofibers are found in the literatures.

Conventionally, $RE_2O_2S:Ln^{3+}$ (RE = Y, La, Gd; Ln = Eu, Tb) luminescent bulk materials were prepared by calcination of the mixture of respective rare-earth oxides [10, 11] or oxalate compounds [19, 20] or carbonates [21, 22], sulfur powders and flux (Na_2CO_3, $Mg_2CO_3{\cdot}4\ Mg(OH)_2{\cdot}5H_2O$, TiO_2) at above 1100 °C for 2 h in a reduced or protective atmosphere. In this way, the morphology of the as-prepared bulk materials is often irregular particles. Even if rare earth oxides nanofibers are applied as precursor, the obtained rare earth oxysulfides do not inherit the peculiar morphologies of rare earth oxides using the above conventional sulfurization method because sulfur powders and flux will melt and destruct the morphologies of rare earth oxides. Therefore, rare earth oxysulfides nanofibers can not be prepared via the above conventional sulfurization method using rare earth oxides nanofibers as precursor.

Electrospinning is a simple, convenient and versatile technique to prepare long fibers with diameters ranging from tens of nanometers up to micrometers, including multifunctional composite nanofibers [23–25], rare earth oxyhalides nanofibers [26–28], metallic oxide and composite oxide nanofibers [29–31], coaxial nanofibers [32, 33], and Janus nanofibers [34–36]. However, to the best of our knowledge, there have been no reports on the preparation of rare earth oxysulfides upconversion luminescence nanofibers by electrospinning combined with sulfurization technique.

In this paper, polyvinyl pyrrolidone (PVP) was selected as template for electrospinning owing to its good solubility, high flexibility, non-toxicity, excellent spinability, easy obtainment, and low costs, etc. $Y_2O_2S:Yb^{3+}$, Er^{3+} nanofibers were fabricated by sulfurization of the relevant $Y_2O_3:Yb^{3+}$, Er^{3+} nanofibers which were prepared by calcination of the electrospun fibers of PVP/[$Y(NO_3)_3$ + $Yb(NO_3)_3$ + $Er(NO_3)_3$] composites. The morphology, structure, upconversion luminescent performance and formation mechanism of $Y_2O_2S:Yb^{3+}$, Er^{3+} nanofibers were systematically studied, and some meaningful results were obtained.

2 Experimental sections

2.1 Chemicals

Polyvinyl pyrrolidone (PVP, Mw = 1300000, AR), yttrium oxide (Y_2O_3, 99.99 %), erbium oxide (Er_2O_3, 99.99 %) and ytterbium oxide (Yb_2O_3, 99.99 %) were purchased from Kemiou Chemical Co. Ltd. *N*,*N*-dimethylformamide (DMF, AR) was bought from Tiantai Chemical Co. Ltd. Nitric acid (AR) and sulfur (AR) were purchased from Beihua Fine Chemical Co. Ltd. All chemicals were directly used as received without further purification.

2.2 Preparation of PVP/[$Y(NO_3)_3$ + $Yb(NO_3)_3$ + $Er(NO_3)_3$] composite nanofibers via electrospinning

Y_2O_2S:10 %Yb^{3+}, x %Er^{3+} [x = 0.5, 1, 2, 3, x stands for molar ratio of Er^{3+} to (Er^{3+} + Yb^{3+} + Y^{3+})] were prepared by a method of electronspinning combined with sulfurization technique. Typical procedure of preparing Y_2O_2S:10 %Yb^{3+}, 2 %Er^{3+} was indicated below. Firstly, rare earth nitrates were prepared by dissolving 0.0241 g of Er_2O_3, 0.1245 g of Yb_2O_3 and 0.6277 g of Y_2O_3 in dilute HNO_3 (1:1, volume ratio) at elevated temperatures, then dissolved in 16.1153 g of DMF, and then 1.8 g of PVP was added into the above solution under stirring for 4 h to form homogeneous transparent spinning solution. In the spinning solution, the mass ratios of rare earth nitrates, DMF and PVP were equal to 9:82:9. Subsequently, the spinning solution was electrospun at room temperature under a positive high voltage of 13 kV, the distance between the spinneret tip and the collector (Al foil) was fixed to 16 cm, and relative humidity was 60–70 %. Thus, PVP/[$Y(NO_3)_3$ + $Yb(NO_3)_3$ + $Er(NO_3)_3$] composite nanofibers were obtained on the collector with the evaporation of DMF.

2.3 Synthesis of $Y_2O_3:Yb^{3+}$, Er^{3+} nanofibers

The as-prepared PVP/[$Y(NO_3)_3$ + $Yb(NO_3)_3$ + $Er(NO_3)_3$] composite nanofibers were annealed at a heating rate of 1 °C/min and remained for 8 h at 700 °C, then the calcination temperature was decreased to 200 °C at a rate of 1 °C/min, and then naturally down to room temperature. Thus, $Y_2O_3:Yb^{3+}$, Er^{3+} nanofibers were obtained.

2.4 Fabrication of $Y_2O_2S:Yb^{3+}$, Er^{3+} nanofibers

Fabrication of $Y_2O_2S:Yb^{3+}$, Er^{3+} nanofibers were performed by Ar gas aided sulfur treatment through calcining $Y_2O_3:Yb^{3+}$, Er^{3+} nanofibers used precursor with sulfur powder as sulfurization agent. Some sulfur powders were put into a small crucible, and carbon rods were loaded on the sulfur powders, $Y_2O_3:Yb^{3+}$, Er^{3+} nanofibers were placed on the carbon rods, then the small crucible was placed into a big crucible, and excess sulfur powders were added into the space between the two crucibles, then the big crucible was covered with its lid. We call this process as a double-crucible method. The crucibles were annealed

at 800 °C for 4 h under Ar gas atmosphere at a heating rate of 5 °C/min, and then the calcination temperature was decreased to 200 °C at a rate of 5 °C/min, followed by down to room temperature naturally, and Y_2O_2S:Yb^{3+}, Er^{3+} nanofibers were successfully acquired.

2.5 Characterization methods

X-ray diffraction (XRD) measurements were performed using a Rigaku D/max-RA XRD diffractometer with Cu Kα radiation of 0.15418 nm, and the operation voltage and current were respectively kept at 40 kV and 20 mA. The size and morphology of the samples were observed by a field emission scanning electron microscope (FESEM, XL-30, FEI Company). The purity of the samples was examined by OXFORD ISIS-300 energy dispersive X-ray spectrometer (EDX). Transmission electron microscopy (TEM) analysis was carried out using a JEM-2010 transmission electron microscope under a working voltage of 200 kV. The up-conversion luminescent spectra of the samples were recorded with a HITACHI F-7000 fluorescence spectrophotometer using a power-tunable 980-nm diode laser as the excitation source.

3 Results and discussion

3.1 XRD analysis

Figure 1 shows the XRD patterns of Y_2O_2S:10 %Yb^{3+} nanofibers doped with different doping concentration of Er^{3+} ions. There are some obvious diffraction peaks near $2\theta = 27.2°$ (100), 30.6° (101), 38.7° (102), 41.1° (003), 48.2° (110), 50.3° (103), 56.1° (112), 58.0° (201), etc. All

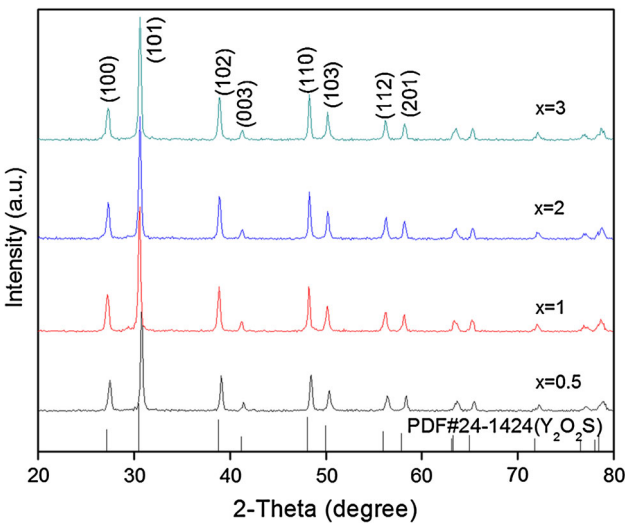

Fig. 1 XRD patters of Y_2O_2S:10 %Yb^{3+}, x %Er^{3+} nanofibers with PDF standard card of Y_2O_2S

the reflection peaks can be perfectly indexed to those of the pure hexagonal phase with primitive structure of Y_2O_2S (PDF#24-1424), and the space group is $P\bar{3}m1$. No diffraction peaks of any other phases or impurities are detected, indicating that the Yb^{3+} and Er^{3+} ions are effectively built into the host lattice via replacing Y^{3+} ions, and the substitution of Y^{3+} with Yb^{3+} and Er^{3+} does not remarkably change the Y_2O_2S host lattice structure.

3.2 SEM, TEM and EDS analysis

Figure 2a shows the typical FESEM image of PVP/[$Y(NO_3)_3$ + $Yb(NO_3)_3$ + $Er(NO_3)_3$] composite nanofibers before calcination, fibers have smooth surface and uniform diameter. After annealing at 700 °C, the diameters of these nanofibers greatly decrease due to loss of the PVP and associated organic components [31], as shown in Fig. 2b, the surface morphology of Y_2O_3:10 %Yb^{3+}, 2 %Er^{3+} nanofibers become rougher than those of the composite nanofibers. FESEM image of Y_2O_2S:10 %Yb^{3+}, 2 %Er^{3+} nanofibers is manifested in Fig. 2c. It reveals that the morphology and diameter of Y_2O_2S:10 %Yb^{3+}, 2 %Er^{3+} nanofibers are nearly similar to those of Y_2O_3:10 %Yb^{3+}, 2 %Er^{3+} nanofibers. Preliminarily, we can safely conclude that the sulfur atmosphere plays an important role in retaining the morphology of the precursor nanofibers. In order to study the diameters distribution of these samples, Image-Pro Plus 6.0 software is used to measure diameters of 100 nanofibers from SEM images, and the results are analyzed with statistics. The histograms of diameters distribution of these fibers are indicated in Fig. 3. It is found from Fig. 3 that under the 95 % confidence level, the diameters of these nanofibers analyzed by Shapiro–Wilk method are normal distribution. The diameters of PVP/[$Y(NO_3)_3$ + $Yb(NO_3)_3$ + $Er(NO_3)_3$] composite nanofibers, Y_2O_3:10 %Yb^{3+}, 2 %Er^{3+} nanofibers and Y_2O_2S:10 %Yb^{3+}, 2 %Er^{3+} nanofibers are 176 ± 26, 134 ± 15 and 105 ± 13 nm, respectively.

TEM image of the Y_2O_2S:10 %Yb^{3+}, 2 %Er^{3+} nanofibers is illustrated in Fig. 4. It is found that the Y_2O_2S:10 %Yb^{3+}, 2 %Er^{3+} nanofibers are composed of nanoparticles with size of 40–70 nm, and the diameter of the Y_2O_2S:10 %Yb^{3+}, 2 %Er^{3+} nanofibers is ca.100 nm. The result is well consistent with that of SEM analysis and further confirms that Y_2O_2S:Yb^{3+}, Er^{3+} nanofibers are successfully prepared.

EDX spectrum of Y_2O_2S:10 %Yb^{3+}, 2 %Er^{3+} nanofibers is manifested in Fig. 5. The presence of Y, O, S, Yb and Er elements corresponds to Y_2O_2S:10 %Yb^{3+}, 2 %Er^{3+} nanofibers and no other impurity elements are found, indicating that the pure Y_2O_2S:Yb^{3+}, Er^{3+} nanofibers are obtained. Au peak is from the conductive film of Au plated on the sample for SEM observation.

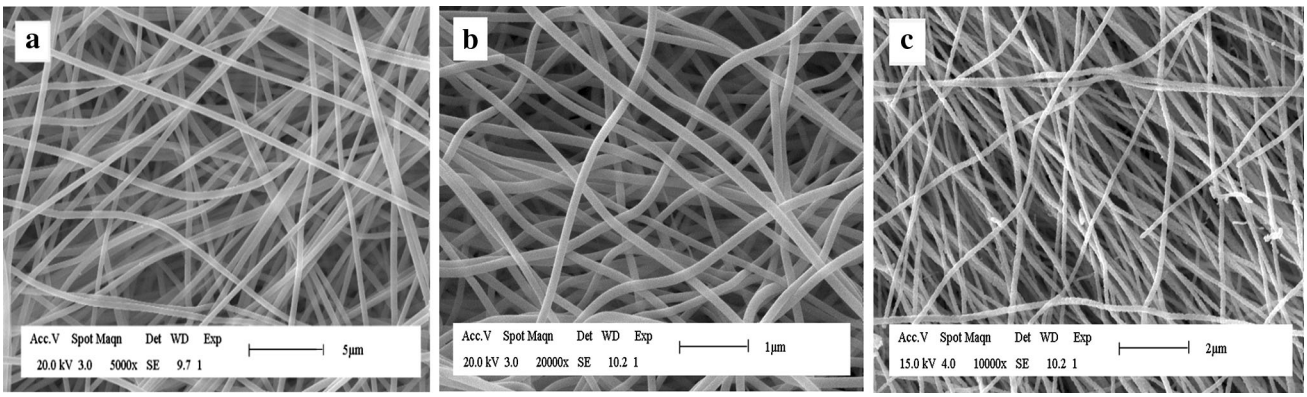

Fig. 2 FESEM images of PVP/[$Y(NO_3)_3$ + $Yb(NO_3)_3$ + $Er(NO_3)_3$] composite fibers (**a**), Y_2O_3:10 %Yb^{3+}, 2 %Er^{3+} nanofibers (**b**) and Y_2O_2S:10 %Yb^{3+}, 2 %Er^{3+} nanofibers (**c**)

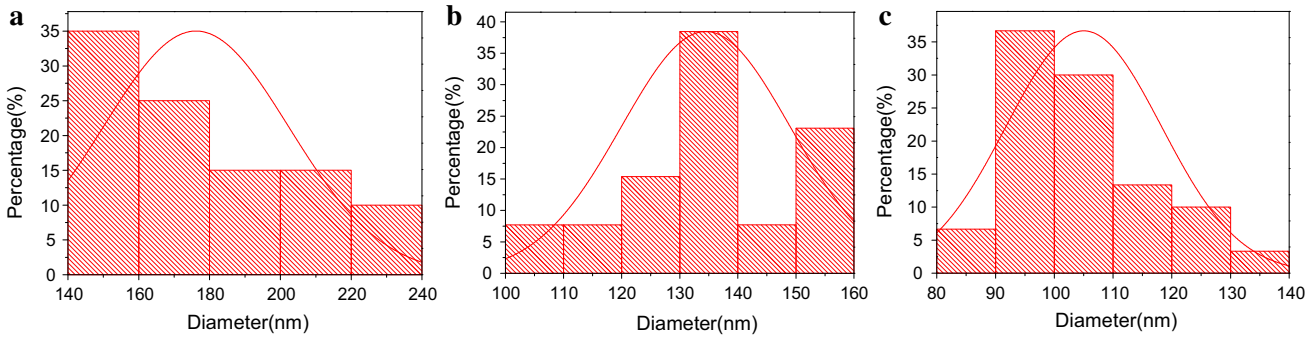

Fig. 3 Histograms of diameters distribution of PVP/[$Y(NO_3)_3$ + $Yb(NO_3)_3$ + $Er(NO_3)_3$] composite fibers (**a**), Y_2O_3:10 %Yb^{3+}, 2 %Er^{3+} nanofibers (**b**) and Y_2O_2S:10 %Yb^{3+}, 2 %Er^{3+} nanofibers (**c**)

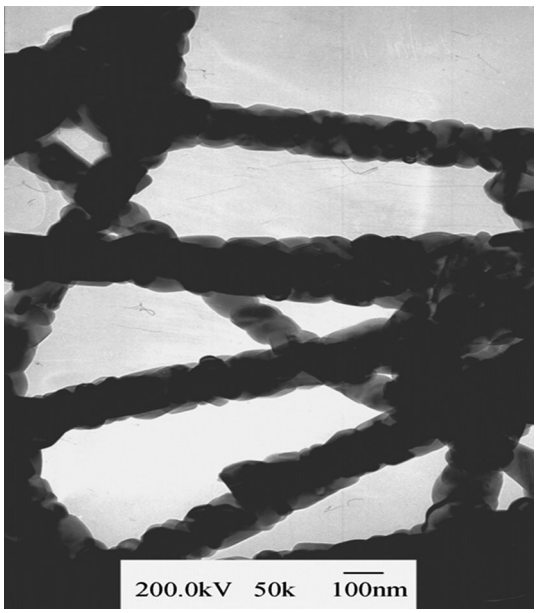

Fig. 4 TEM image of Y_2O_2S:10 %Yb^{3+}, 2 %Er^{3+} nanofibers

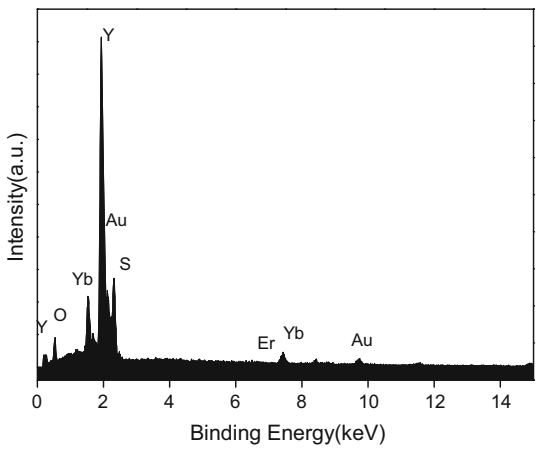

Fig. 5 EDX spectrum of Y_2O_2S:10 %Yb^{3+}, 2 %Er^{3+} nanofibers

3.3 Up-conversion luminescent characteristics

Upon the excitation of a 980-nm diode laser, up-conversion emission spectra of Y_2O_2S:10 %Yb^{3+} nanofibers doped with different concentration of Er^{3+} ions are obtained, as

shown in Fig. 6. The nanofibers emit strong green and weak red up-conversion emissions centering at 526, 548 and 668 nm, respectively. The strong green emissions are respectively assigned to the $^2H_{11/2} \rightarrow {}^4I_{15/2}$ and $^4S_{3/2} \rightarrow {}^4I_{15/2}$ energy levels transitions of Er^{3+}, and the red emission is attributed to the transitions of $^4F_{9/2} \rightarrow {}^4I_{15/2}$ energy levels of Er^{3+} ions. The comparison among the up-conversion luminescence spectra of these nanofibers shows that the intensity of the green up-conversion luminescence is increased more than that of the red one, and the relative intensity ratio I_{green}/I_{red} (ca. 2, 2.11, 2.67 and 3.46 for Er^{3+}-doping concentration of 0.5, 1, 2 and 3 %, respectively) increases with the increase of Er^{3+} concentration. When the Er^{3+} concentration is higher than 2 %, the concentration quenching effect occurs and thus the luminescence intensity is decreased. Therefore, the optimum molar ration of Yb^{3+} to Er^{3+} in the $Y_2O_2S:Yb^{3+}$, Er^{3+} nanofibers is 5:1.

In the upconversion (UC) emission process, the UC emission intensity (I_{up}) is proportional to the *n* power of the pump power (P) according to the following formula [37, 38]: $I_{up} \propto P^n$, Where n is the number of infrared photons required to absorb for emitting one visible photon. The pump power dependence of the visible emission bands was measured in these samples. A plot of natural logarithm I_{up} versus natural logarithm P yields a straight line with slope n, as shown in Fig. 7. It is seen that the luminescence intensities of both green and red up-conversion increase with the increase of the pump powers. For the green (548 nm) and red (668 nm) emissions, the values of n (the slope) for $^4S_{3/2} \rightarrow {}^4I_{15/2}$ (548 nm) and $^4F_{9/2} \rightarrow {}^4I_{15/2}$ (668 nm) energy levels transitions of Er^{3+} ions in $Y_2O_2S:Yb^{3+}$, Er^{3+} nanofibers are determined to be 1.82 and 1.99, respectively. Generally, a straight line with the slope approximately equal to 2 for the up-conversion luminescence indicates two photons involve in this up-conversion luminescence process. From the above results, it is proved that both the green and red emissions of $Y_2O_2S:Yb^{3+}$, Er^{3+} nanofibers are two-photon process.

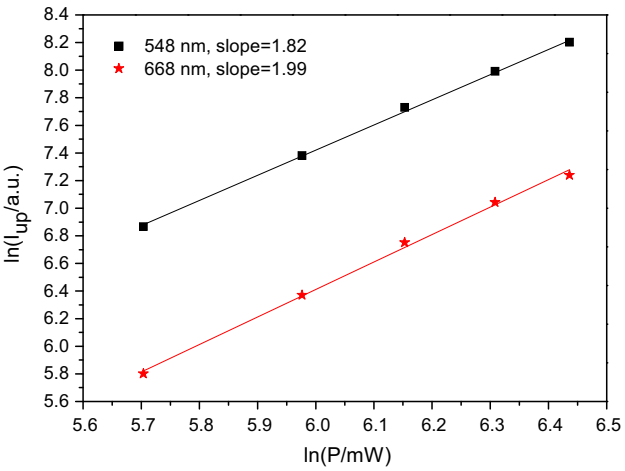

Fig. 7 Plots of natural logarithm intensity of the up-conversion emission versus natural logarithm pumped power

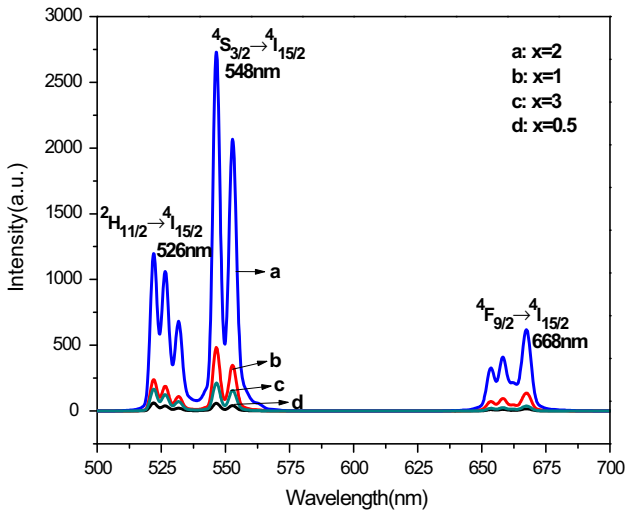

Fig. 6 Up-conversion emission spectra of Y_2O_2S:10 %Yb^{3+}, x %Er^{3+} nanofibers excited by a 980-nm diode laser

In principle, four basic population mechanisms may be involved in the UC process, namely energy transfer (ET), ground state absorption (GSA), excited state absorption (ESA) and photo avalanche (PA) [39]. We can immediately rule out PA as a mechanism of up-conversion in $Y_2O_2S:Yb^{3+}$, Er^{3+} nanofibers because no inflection point is observed in the power study. The two-photon process in $Y_2O_2S:Yb^{3+}$, Er^{3+} nanofibers may happen via the following GSA, ESA and ET processes and their possible schematic diagram is shown in Fig. 8 [32]. When the Yb^{3+} and Er^{3+} ions are co-doped into the host lattices, the ET process become dominant because Yb^{3+} ion has a much larger absorption cross section as compared with that of Er^{3+} around 980 nm [39]. Therefore, the Er^{3+} ions are excited from the ground state to $^4I_{11/2}$ level by general multi-photon processed through the ET from the excited Yb^{3+} ions [$^4I_{15/2}$ (Er) + $^2F_{5/2}$ (Yb) $\rightarrow$ $^4I_{11/2}$ (Er) + $^2F_{7/2}$ (Yb)]. Then the ions in $^4I_{11/2}$ level are raised to $^4F_{7/2}$ level via the ESA or the ET from Yb^{3+} ions to the excited Er^{3+} ions. The electrons in $^4F_{7/2}$ level undergo multi-photon relaxation to the luminescent level $^2H_{11/2}$ and $^4S_{3/2}$ resulting from the small energy gap between them. The radiative transition from $^2H_{11/2}$ and $^4S_{3/2}$ to ground state can result in the green emissions at 526 and 548 nm. For the red emissions at 668 nm, the electrons at the excited state $^4I_{11/2}$ relax nonradiatively to the $^4I_{13/2}$ level, then the electrons at $^4I_{13/2}$ level can be excited to the $^4F_{9/2}$ level by the ESA or ET processes from Yb^{3+}. The red emission at 668 nm originates from the transition from the $^4F_{9/2}$ to $^4I_{15/2}$.

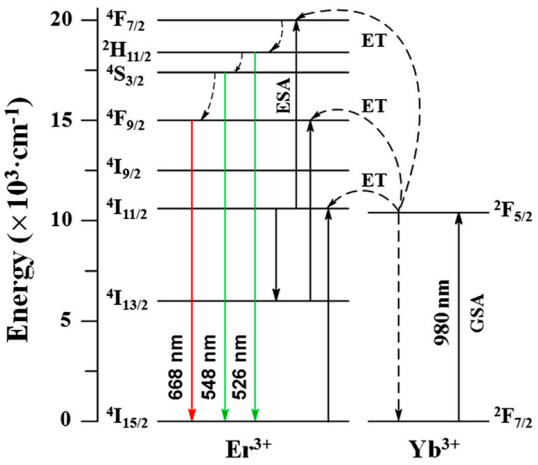

Fig. 8 Up-conversion mechanism and population processes in Yb^{3+} and Er^{3+} co-doped Y_2O_2S nanofibers

3.4 Possible formation mechanism for the $Y_2O_2S:Yb^{3+}$, Er^{3+} nanofibers

Possible formation mechanism of $Y_2O_2S:Yb^{3+}$, Er^{3+} nanofibers is shown in Fig. 9. PVP, $Y(NO_3)_3$,$Yb(NO_3)_3$ and $Er(NO_3)_3$ are mixed with DMF to form spinning solution. Y^{3+}, Yb^{3+}, Er^{3+}, NO_3^- are mixed or absorbed onto PVP to form sol with certain viscosity, then PVP/$[Y(NO_3)_3 + Er(NO_3)_3 + Yb(NO_3)_3]$ composite nanofiber are fabricated under electrospinning. PVP acts as template during the formation of $Y_2O_3:Yb^{3+}$, Er^{3+} nanofibers. In the process of calcination, PVP is oxidized to break the chain, and then to volatilize. Nitrates are decomposed and oxidized to produce NO_2, and Y^{3+}/Yb^{3+}/Er^{3+} are oxidized to form $Y_2O_3:Yb^{3+}$, Er^{3+} crystallites, many crystallites are combined into nanofiber. Then, $Y_2O_3:Yb^{3+}$, Er^{3+} nanofiber is sulfurized using S powers as sulfurization agent. In the sulfurization process, S is gasificated at about 350 °C. With the increase of calcination temperature, gasificated sulfur reacts with $Y_2O_3:Yb^{3+}$, Er^{3+} nanofibers to produce $Y_2O_2S:Yb^{3+}$, Er^{3+} nanofibers. During the process, sulfur powders and $Y_2O_3:Yb^{3+}$, Er^{3+} nanofibers are separated by carbon rods which prevent $Y_2O_3:Yb^{3+}$, Er^{3+} nanofibers from morphology damage and also play a key role in reduction through reacting with oxygen species of $Y_2O_3:Yb^{3+}$, Er^{3+} in the heating process. The double-crucible method we proposed here is actually a solid–gas reaction, which has been proved to be an important method, not only can retain the morphology of $Y_2O_3:Yb^{3+}$, Er^{3+} nanofibers, but also can fabricate $Y_2O_2S:Yb^{3+}$, Er^{3+} nanofibers with pure phase at relatively low temperature. Reaction schemes for formation of $Y_2O_2S:Yb^{3+}$, Er^{3+} nanofibers proceed as follows:

$$\mathrm{PVP}/\left[\mathrm{Y(NO_3)_3} + \mathrm{Yb(NO_3)_3} + \mathrm{Er(NO_3)_3}\right] + \mathrm{O_2} \overset{700^\circ\mathrm{C}}{\rightarrow} \mathrm{CO_2} + \mathrm{H_2O} + \mathrm{NO_2} + \mathrm{Y_2O_3{:}Yb^{3+},Er^{3+}}$$

$$\mathrm{Y_2O_3{:}Yb^{3+},\ Er^{3+}} + \mathrm{S} + \mathrm{C} \overset{800^\circ\mathrm{C}}{\rightarrow} \mathrm{Y_2O_2S{:}Yb^{3+},\ Er^{3+}} + \mathrm{CO}$$

$$\mathrm{Y_2O_3{:}Yb^{3+},\ Er^{3+}} + \mathrm{S} + \mathrm{CO} \overset{800^\circ\mathrm{C}}{\rightarrow} \mathrm{Y_2O_2S{:}\ Yb^{3+},\ Er^{3+}} + \mathrm{CO_2}$$

4 Conclusions

In summary, pure hexagonal phase $Y_2O_2S:Yb^{3+}$, Er^{3+} nanofibers with space group $P\bar{3}m1$were fabricated via sulfurization of the electrospinning-derived cubic-phase $Y_2O_3:Yb^{3+}$, Er^{3+} nanofibers. The morphology of $Y_2O_3:Yb^{3+}$, Er^{3+} nanofibers can be inherited to

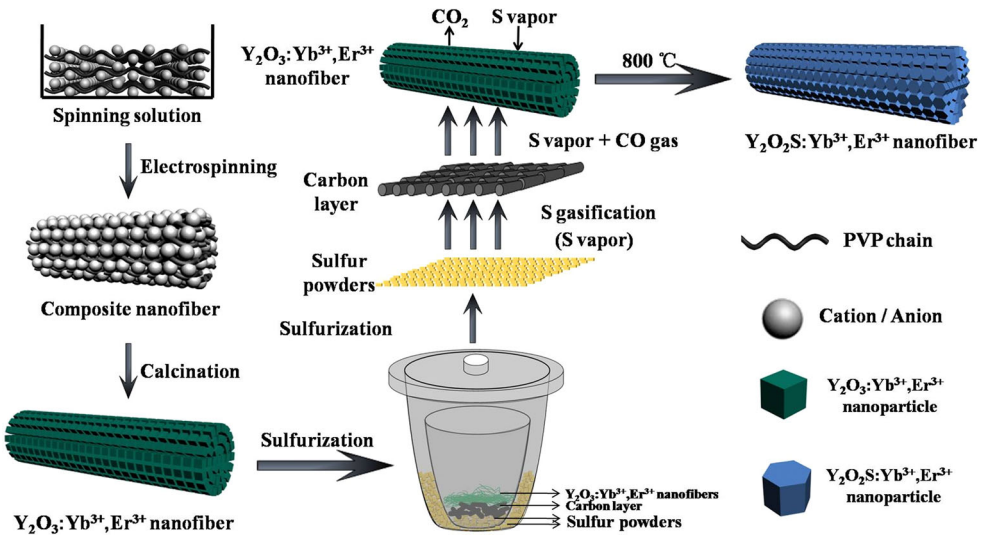

Fig. 9 Possible formation mechanism of $Y_2O_2S:Yb^{3+}$, Er^{3+} nanofibers

$Y_2O_2S:Yb^{3+}$, Er^{3+} using sulfur powders as sulfurization reagent via the double-crucible method. The diameters of $Y_2O_2S:Yb^{3+}$, Er^{3+} nanofibers analyzed by Shapiro–Wilk method are normal distribution and are 105 ± 13 nm. Upon the excitation of a 980-nm diode laser, $Y_2O_2S:Yb^{3+}$, Er^{3+} nanofibers emit green and red up-conversion emissions centering at 526, 548 and 668 nm, respectively attributed to the $^2H_{11/2}/^4S_{3/2} \rightarrow {}^4I_{15/2}$ and $^4F_{9/2} \rightarrow {}^4I_{15/2}$ energy levels transitions of Er^{3+} ions. The double-crucible sulfurization technique we propose here is of universal importance to fabricate other rare earth oxysulfide nanomaterials with various morphologies.

Acknowledgments This work was financially supported by the National Natural Science Foundation of China (NSFC 50972020, 51072026), Specialized Research Fund for the Doctoral Program of Higher Education (20102216110002, 20112216120003), the Science and Technology Development Planning Project of Jilin Province (Grant Nos. 20130101001JC, 20070402), the Science and Technology Research Project of the Education Department of Jilin Province during the eleventh five-year plan period (Under grant No. 2010JYT01).

References

1. M. Mikami, A. Oshiyama, Phys. Rev. B **57**, 8939–8944 (1998)
2. T. Jűstel, H. Nikol, C. Ronda, Angew. Chem. Int. Ed. **37**, 3084–3103 (1998)
3. J.B. Lian, X.D. Sun, J.G. Li, X.D. Li, Opt. Mater. **33**, 596–600 (2011)
4. F. Wang, B. Yang, J.C. Zhang, Y.N. Dai, W.H. Ma, J. Lumin. **130**, 473–477 (2010)
5. A.M. Pires, O.A. Serra, M.R. Davolos, J. Alloys Compd. **374**, 181–184 (2004)
6. P.F. Ai, W.Y. Li, L.Y. Xiao, Y.D. Li, H.J. Wang, Y.L. Liu, Ceram. Int. **36**, 2169–2174 (2010)
7. Y. Fu, W.H. Cao, Y. Peng, X.X. Luo, M.M. Xing, J. Mater. Sci. **45**, 6556–6561 (2010)
8. Y. Jiang, Y. Wu, Y. Xie, Y.T. Qian, J. Am. Ceram. Soc. **83**, 2628–2630 (2000)
9. C.L. Lo, J.G. Duh, B.S. Chiou, C.C. Peng, L. Ozawa, Mater. Chem. Phys. **71**, 179–189 (2001)
10. T.M. Chou, S. Mylswamy, R.S. Liu, S.Z. Chuang, Solid State Commun. **136**, 205–209 (2005)
11. P. Huang, F. Yang, L. Wang, X. Lei, Ceram. Int. **39**, 5615–5621 (2013)
12. Q.L. Dai, H.W. Song, M.Y. Wang, X. Bai, B. Dong, R.F. Qin, X.S. Qu, H. Zhang, J. Phys. Chem. C **112**, 19399–19404 (2008)
13. Y.Y. Li, D.C. Dai, S.H. Cai, J. Chin. Soc. Rare Earths **14**, 16–20 (1996)
14. H. Kim, D.W. Hang, J.S. Lee, J. Am. Chem. Soc. **126**, 8912–8913 (2004)
15. Y.H. Song, H.P. You, Y.J. Huang, M. Yang, Y.H. Zheng, L.H. Zhang, N. Guo, Inorg. Chem. **49**, 11499–11504 (2010)
16. W.Y. Li, Y.L. Liu, P.F. Ai, X.B. Chen, J. Rare Earths **27**, 895–899 (2009)
17. J. Thirumalai, R. Chandramohan, T.A. Vijayan, R.M. Somasundaram, Mater. Res. Bull. **46**, 285–291 (2011)
18. J.F. Jonhson, J.E. Geusic, H.J. Guggenheim, T. Kushida, S. Singh, L.G. Van Uiter, Appl. Phys. Lett. **15**, 48–50 (1969)
19. D.C. Hanna, R.M. Percival, I.R. Perry, Opt. Commun. **78**, 187–194 (1990)
20. D.Q. Chen, Y.S. Wang, K.L. Zheng, T.L. Guo, Y.L. Yu, P. Huang, Opt. Lett. **33**, 1884–1886 (2008)
21. S. Sivakumar, F.C.J.M. Van Veggel, M. Raudsepp, J. Am. Chem. Soc. **127**, 12464–12465 (2005)
22. R. Martín-Rodríguez, R. Valiente, C. Pesquera, F. González, C. Blanco, V. Potin, M.C. Marcode Lucas, J. Lumin. **129**, 1109–1114 (2009)
23. S.J. Sheng, Q.L. Ma, X.T. Dong, N. Lv, J.X. Wang, W.S. Yu, G.X. Liu, J. Mater. Sci. Mater. Electron. **25**, 1309–1316 (2014)
24. D.D. Yin, Q.L. Ma, X.T. Dong, N. Lv, J.X. Wang, W.S. Yu, G.X. Liu, J. Mater. Sci. Mater. Electron. (2015). doi:10.1007/s10854-015-2741-9
25. K. Lun, Q.L. Ma, X.T. Dong, W.S. Yu, J.X. Wang, G.X. Liu, J. Mater. Sci. Mater. Electron. **25**, 5395–5402 (2014)
26. H.Y. Wang, Y. Yang, Y. Wang, Y.Y. Zhao, X. Li, C. Wang, J. Nanosci. Nanotechnol. **9**, 1522–1525 (2009)
27. D. Li, X.T. Dong, W.S. Yu, J.X. Wang, G.X. Liu, J. Mater. Sci. Mater. Electron. **24**, 3041–3048 (2013)
28. S. Wu, X.T. Dong, J.X. Wang, Q.L. Kong, W.S. Yu, G.X. Liu, J. Mater. Sci. Mater. Electron. **25**, 1053–1062 (2014)
29. M.Y. Zhang, C.L. Shao, J.B. Mu, X.M. Huang, Z.Y. Zhang, Z.C. Guo, P. Zhang, Y.C. Liu, J. Mater. Chem. **22**, 577–584 (2012)
30. Z.Y. Zhang, C.L. Shao, X.H. Li, Y.Y. Sun, M.Y. Zhang, J.B. Mu, P. Zhang, Z.C. Guo, Y.H. Liu, Nanoscale **5**, 606–618 (2013)
31. X.T. Dong, L. Liu, J.X. Wang, G.X. Liu, Chem. J. Chin U. **31**, 20–25 (2010)
32. X. Bai, H.W. Song, G.H. Pan, X.G. Ren, B. Dong, Q.L. Dai, L.B. Fan, J. Nanosci. Nanotechnol. **9**, 2677–2681 (2009)
33. Q.L. Ma, J.X. Ma, X.T. Wang, WSYu. Dong, G.X. Liu, J. Xu, J. Mater. Chem. **22**, 14438–14442 (2012)
34. N. Lv, Q.L. Ma, X.T. Dong, J.X. Wang, W.S. Yu, G.X. Liu, ChemPlusChem **79**, 690–697 (2014)
35. F. Bi, X.T. Dong, J.X. Wang, G.X. Liu, RSC Adv. **5**, 12571–12577 (2015)
36. X. Xi, J.X. Wang, X.T. Dong, Q.L. Ma, W.S. Yu, G.X. Liu, Chem. Eng. J. **254**, 259–267 (2014)
37. G.S. Yi, B.Q. Sun, F.Z. Yang, D.P. Chen, Y.X. Zhou, J. Cheng, Chem. Mater. **14**, 2910–2914 (2002)
38. M. Pollnau, D.R. Gamelin, S.R. Luthi, H. Gudel, Phys. Rev. B **61**, 3337–3346 (2000)
39. Y.H. Song, Y.J. Huang, L.H. Zhang, Y.H. Zheng, N. Guo, H.P. You, RSC Adv. **2**, 4777–4781 (2012)